SUPPORTING INFORMATION

Hypersaline Electrodialysis Desalination: Intrinsic Membrane and Module Performance Tradeoffs

ACS ES&T Engineering

Hanqing Fan[†,‡], Yuxuan Huang[†], Peter Cruz-Grace[†], and Ngai Yin Yip[*,†,§]

[†] Department of Earth and Environmental Engineering, Columbia University, New York, New York 10027-6623, United States

[‡] Department of Chemical and Environmental Engineering, Yale University, New Haven, Connecticut 06520-8286, United States

[§] Columbia Water Center, Columbia University, New York, New York 10027-6623, United States

[*] Corresponding author: Email: n.y.yip@columbia.edu, Phone: +1 212 8542984

Number of Pages: 24

Number of Figures: 6

Number of Tables: 2

MEMBRANE- AND MODULE-SCALE TRANSPORT MODELS

Ion Partitioning. Counter- and co-ion equilibrium concentrations at the membrane-solution interfaces are described using the Donnan-Manning model.[1,2] As the electrochemical potentials are equal (Figure S1 and Figure 1C of the main manuscript), the concentrations of counter- and co-ions in the membrane and bulk solution can be related to the electrical potential difference across the solution-membrane interface, termed the Donnan potential, $\Delta\varphi_{\text{Donnan}}$:[3]

$$\frac{R_g T}{z_{ct} F}\ln\left(\frac{\gamma_{ct}^{m} c_{ct}^{m}}{f_w \gamma_{ct}^{s} c_{ct}^{s}}\right) = \frac{R_g T}{z_{co} F}\ln\left(\frac{\gamma_{co}^{m} c_{co}^{m}}{f_w \gamma_{co}^{s} c_{co}^{s}}\right) = -\Delta\varphi_{\text{Donnan}} \tag{S1}$$

where γ is activity coefficient, c is molar concentration, z is ion valence, f_w is volume fraction of water, R_g is the gas constant, F is the Faraday constant, and T is absolute temperature. Superscripts s and m denote the bulk solution and membrane phases, respectively, whereas subscripts ct and co signify counter- and co-ion.

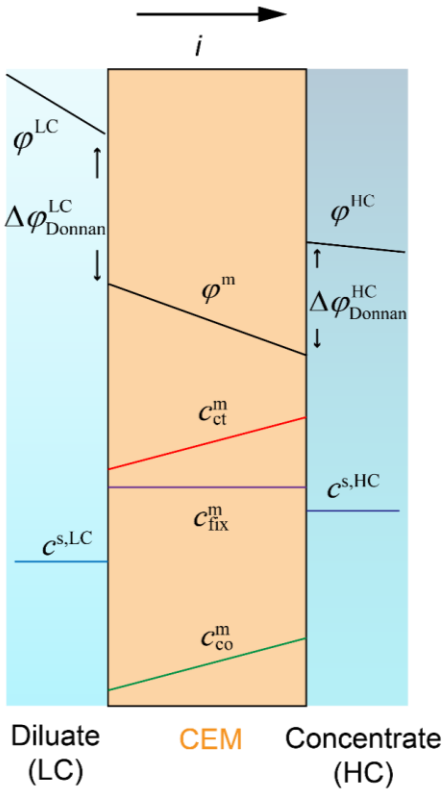

Figure S1. Schematic depicting concentration, c, and electric potential, φ, profiles across an IEM in ED (with CEM as an illustrative example). The low-concentration diluate stream and the high-concentration

concentrate stream are denoted by superscripts LC and HC, respectively, whereas the bulk solutions are represented by superscript s. Membrane concentrations (designated by superscript m) of counterion, co-ion, and fixed charge density are indicated by c_{ct}^{m}, c_{co}^{m}, and c_{fix}^{m}, respectively (i.e., subscripts of ct, co, and fix). The applied current density and electric potential are *i* and φ, respectively. Electric potentials of the bulk solutions are φ^{LC} and φ^{HC}, Donnan potentials at membrane-solution interfaces are $\Delta\varphi_{Donnan}^{LC}$ and $\Delta\varphi_{Donnan}^{HC}$, and potential within the membrane is φ^{m}.

Activity coefficients in the bulk solution, γ^{s}, can be determined using activity models. In this study, the Pitzer equations are employed to simulate γ^{s} because of their suitability for very high ionic strength environments.[4,5] The parameters of NaCl in the original papers of Pitzer et al. were adopted.[4,5] The relationship between activity coefficient and molar concentration of NaCl is presented in Figure S2 of the Supporting Information.

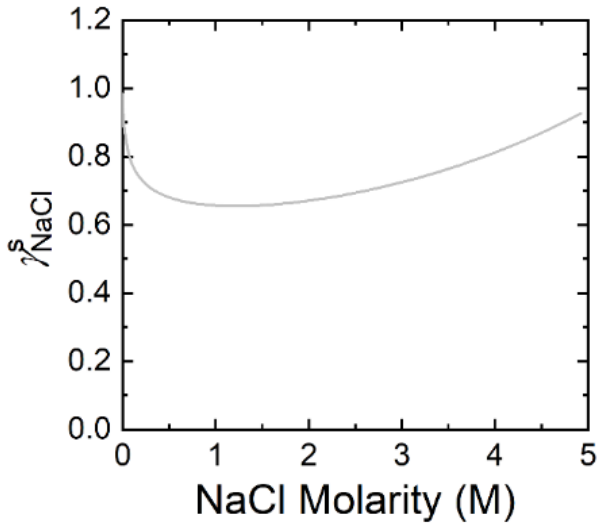

Figure S2. NaCl activity coefficient as a function of NaCl molar concentration in bulk aqueous solution.

Activity coefficients in the membrane phase, γ^{m}, are evaluated using the counterion condensation theory.[1,2,6] Additionally, electroneutrality in the membrane needs to be maintained, dictating that

$$z_{ct}c_{ct}^{m} + z_{co}c_{co}^{m} + z_{fix}c_{fix}^{m} = 0 \qquad \text{(S2)}$$

where $c_{\mathrm{fix}}^{\mathrm{m}}$ is membrane fixed charge density (normalized by wet volume). $c_{\mathrm{ct}}^{\mathrm{m}}$ and $c_{\mathrm{co}}^{\mathrm{m}}$ can then be established by simultaneously satisfying eqs S1 and S2. Because γ^{s} and γ^{m} are nonlinear functions of c^{s} and c^{m}, respectively, an iterative method is used to solve the system of equations.

Ion Diffusivity (Mobility). Counter- and co-ions diffusivities (for 1:1 electrolytes, e.g., NaCl) in IEMs, $D_{\mathrm{ct}}^{\mathrm{m}}$ and $D_{\mathrm{co}}^{\mathrm{m}}$, respectively, are simulated by the Mackie-Meares spatial model and the counterion condensation theory:[7]

$$D_{\mathrm{ct}}^{\mathrm{m}} = f_{\mathrm{u}} D_{\mathrm{ct,u}}^{\mathrm{m}} + \left(1 - f_{\mathrm{u}}\right) D_{\mathrm{ct,c}}^{\mathrm{m}} \tag{S3a}$$

$$D_{\mathrm{ct,u}}^{\mathrm{m}} = D_{\mathrm{ct}}^{\mathrm{s}} \left(\frac{f_{\mathrm{w}}}{2 - f_{\mathrm{w}}} \right)^2 \left(1 - \frac{1}{3} A\left(1; \frac{X}{\xi}\right) \right) \tag{S3b}$$

$$D_{\mathrm{co}}^{\mathrm{m}} = D_{\mathrm{co}}^{\mathrm{s}} \left(\frac{f_{\mathrm{w}}}{2 - f_{\mathrm{w}}} \right)^2 \left(1 - \frac{1}{3} A\left(1; \frac{X}{\xi}\right) \right) \tag{S3c}$$

where D^{s} is aqueous diffusivity in infinitely dilute solutions,[8] subscripts u and c in $D_{\mathrm{ct}}^{\mathrm{s}}$ denote uncondensed and condensed phases, respectively, f_{u} is fraction of counterions in the membrane that are uncondensed, X is ratio of fixed charge density to membrane co-ion concentration (i.e., $c_{\mathrm{fix}}^{\mathrm{m}} / c_{\mathrm{co}}^{\mathrm{m}}$), and A is a function for the electrostatic effect on diffusivity. Details of the method to determine f_{u} and A can be found in literature.[7,9] ξ is the Manning parameter:

$$\xi = \frac{e^2}{4\pi\varepsilon_0 \varepsilon_r k_{\mathrm{B}} T b} \tag{S4}$$

where b is distance between fixed charges on the polymer chain, e is the elementary charge, ε_0 is the permittivity of vacuum, ε_r is dielectric constant, and k_{B} is the Boltzmann constant. In this study, ε_r is estimated as the volume-weighted average of polymer and water dielectric constants.[7] In this modeling analysis, we estimated b based on the charge density, volume fraction of water, and the Avogadro constant, N_{A}, assuming the charge groups distributed relatively even in the water phase:

$$b = \left(\frac{f_{\mathrm{w}}}{c_{\mathrm{fix}}^{\mathrm{m}} N_{\mathrm{A}}} \right)^{\frac{1}{3}} \tag{S5}$$

Condensed counterion diffusivity, $D_{\mathrm{ct,c}}^{\mathrm{m}}$, is characterized using the reported results of a previous study,[7] which observed the condensed phase diffusivity to be 2–2.5× the uncondensed phase diffusivity in electro-migration. The average of the reported experimental results is used in this analysis: $D_{\mathrm{ct,c}}^{\mathrm{m}} = 2.26 D_{\mathrm{ct,u}}^{\mathrm{m}}$. A recent study presented a theoretical transport framework to model the mobility of condensed counterions.[10] The transport model slightly overpredicts the overall conductivity contribution from counterions, but the disagreements are severely exacerbated at high salinities (results not shown), yielding modeled electrodialysis desalination performance that is exceedingly enhanced (e.g., improbably high permselectivities and unrealistically low energy consumptions). As such, the experimentally-supported condensed phase diffusivity mentioned above was employed in this study over the analytic model.

Membrane Conductivity and Permselectivity. IEM conductivity, σ^{m}, characterizes the ability of the membrane to conduct ions and is[11]

$$\sigma^{\mathrm{m}} = \frac{F^2}{R_{\mathrm{g}} T} \sum z_i^2 c_i^{\mathrm{m}} D_i^{\mathrm{m}} \tag{S6}$$

The selectivity of IEMs for counterions as the primary current carriers rather than co-ions determines the current efficiency. In practice, the undesired leakage of co-ions is inherently unavoidable and is especially exacerbated in hypersaline desalination.[6,9] Membrane permselectivity, α, quantifies the preferential transport of counterions and, thus, describes the IEM ability to suppress co-ion leakage:[3]

$$\alpha = \frac{T_{\mathrm{ct}}^{\mathrm{m}} - T_{\mathrm{ct}}^{\mathrm{s}}}{T_{\mathrm{co}}^{\mathrm{s}}} \tag{S7}$$

where transport number, T, is the fraction of total ionic current carried by the counter- or co-ions.[3] Transport number in solution phase, T_i^{s}, is $z_i^2 D_i^{\mathrm{s}} c_i^{\mathrm{s}} \big/ \sum z_j^2 D_j^{\mathrm{s}} c_j^{\mathrm{s}}$ and transport numbers in membrane phase, T_i^{m}, are determined by the fluxes (eq 1 of the main manuscript): $z_i J_i \big/ \sum z_j J_j$.

Osmotic Water Permeability. Osmotic water transport is described by eq 2 of the main manuscript: $J_{\mathrm{w}}^{\mathrm{O}} = P_{\mathrm{w}}^{\mathrm{O}} \left(\Delta\pi / \Delta x^{\mathrm{m}} \right)$, where $J_{\mathrm{w}}^{\mathrm{O}}$ is water flux, $P_{\mathrm{w}}^{\mathrm{O}}$ is osmotic water permeability of the membrane, $\Delta\pi$ is osmotic pressure difference across the IEM, and Δx^{m} is membrane

thickness. Compared to $\Delta\pi$, hydraulic pressure differences across the membrane from fluid circulation are small. Therefore, this analysis does not include water flux from external hydraulic pressures. We employed a semi-empirical relationship between P_w^O and free volume in the membrane:[12]

$$\ln(P_w^O) = -n_2\left[x(1-n_1)/(1+n_1x)\right] - \ln(1+x) + n_3 \quad \text{(S8)}$$

where $x = [1-f_w]/f_w$, f_w is volume fraction of water, and n_1, n_2, and n_3 are fitting parameters.

Regressing literature data of ion-exchange and highly charged membranes on eq S8 yields values of 0.3995, 2.850, and 3.029 for the fitting parameters n_1, n_2, and n_3, respectively (Figure S3),[13–19] thus establishing P_w^O as a semi-empirical function of f_w in the simulations of this study.

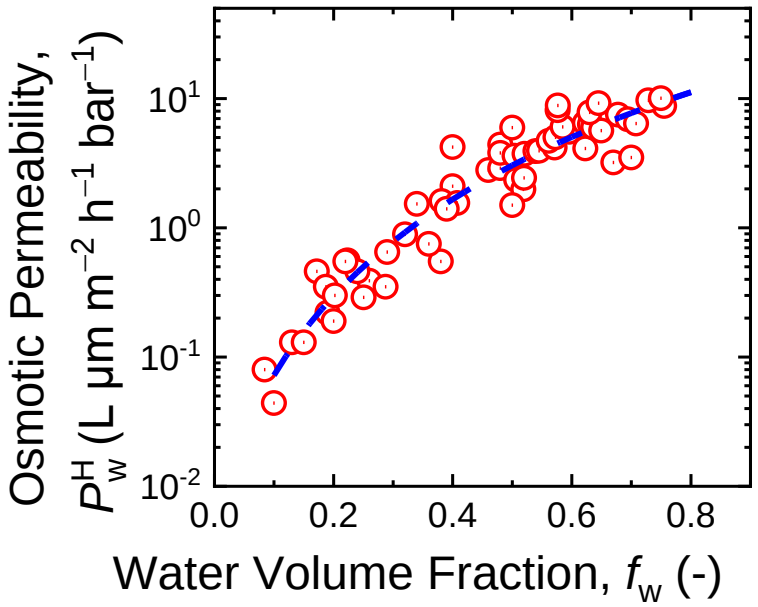

Figure S3. Osmotic water permeability, P_w^O, as a function of membrane water volume fraction, f_w. Blue dashed line is the regression of eq S8 on literature data (red circle symbols)[13–19] with n_1, n_2, and n_3 as fitting parameters.

Electro-Osmotic Water Permeability. P_w^E of 7.12×10^{-10} m^3 A^{-1} s^{-1} was adopted for all simulations, averaged from reported values in a previous study.[20]

Electric Potential Drops. Under constant current density, i, voltage drops, $\Delta\varphi$, across the diluate and concentrate channels can be expressed using Ohm's law:

$$\Delta\varphi^{\mathrm{LC/HC}} = -\frac{i}{\sigma^{\mathrm{LC/HC}}}\Delta x^{\mathrm{LC/HC}} \tag{S9}$$

where $\sigma^{\mathrm{LC/HC}}$ is solution ionic conductivity and $\Delta x^{\mathrm{LC/HC}}$ is channel thickness (superscript LC/HC indicates low/high concentration stream). The solution ionic conductivity, $\sigma^{\mathrm{LC/HC}}$ (in mS/cm), is calculated using the bulk solution concentration, $c^{\mathrm{LC/HC}}$ (in M): $-8.16\times c^2+88.8\times c+2.94$ for $c^{\mathrm{LC/HC}} >$ 1.0 M or $-15.5\times c^2+101\times c+0.168$ for $c^{\mathrm{LC/HC}} <$ 1.0 M. The empirical relationships are established using experimental characterizations of solution conductivity (with a conductivity meter, Orion Star, Thermo Fisher, Waltham, MA). Electric potential differences across the IEMs, $\Delta\varphi^{\mathrm{CEM}}$ and $\Delta\varphi^{\mathrm{AEM}}$ (superscripts denote cation and anion exchange membranes), are the net of the two interfacial Donnan potentials, $\Delta\varphi_{\mathrm{Donnan}}$, on either side of the membrane and the transmembrane ohmic potential change, $\Delta\varphi^{\mathrm{m}}$ (Figure S1 and Figure 1C of the main manuscript):

$$\Delta\varphi^{\mathrm{CEM/AEM}} = \Delta\varphi_{\mathrm{Donnan}}^{\mathrm{CEM/AEM,LC}} + \Delta\varphi^{\mathrm{CEM/AEM,m}} - \Delta\varphi_{\mathrm{Donnan}}^{\mathrm{CEM/AEM,HC}} \tag{S10}$$

$\Delta\varphi_{\mathrm{Donnan}}$ is described by eq S1 and $\Delta\varphi^{\mathrm{m}}$ can be determined by Nernst-Planck analysis of ion transport, i.e., eq 1 of the main manuscript.

Constituents of Energy Consumption. Specific energy consumption normalized by mass of salts separated from the initial saline feed, SEC_s, can be further decomposed into four constituents: 1) work required to overcome the Donnan potentials, 2) membrane ohmic loss, 3) channel ohmic loss, and 4) current efficiency loss. The applied current density, i, consists of counterion fluxes and undesired co-ion leakages. First, we define i_{eff} as the effective electric current density driving the net ion flux from diluate to concentrate For cation, i_{eff} is the counterion flux in the CEM subtracted by the co-ion flux in the AEM (for a simple symmetric salt, the net anion flux has the same value due to charge neutrality). i_{eff} can be expressed as

$$i_{\mathrm{eff}} = z_{\mathrm{ct}}^{\mathrm{CEM}}\left(J_{\mathrm{ct}}^{\mathrm{CEM}} - J_{\mathrm{co}}^{\mathrm{AEM}}\right)F \tag{S11}$$

Eq S11 describes i_{eff} with cation (Na^+ in this study) fluxes. The anionic form of eq S11, $z_{\mathrm{ct}}^{\mathrm{AEM}}\left(J_{\mathrm{ct}}^{\mathrm{AEM}} - J_{\mathrm{co}}^{\mathrm{CEM}}\right)F$, yields the same value due to charge balance. The energy cost for effectively driving ions against the Donnan potentials ($\sum\Delta\varphi_{\mathrm{Donnan}}$) at membrane-solution interfaces, SEC_s-DP, can be then calculated as

$$SEC_{\mathrm{s}}\text{-DP}=\frac{\left|\int_0^{t_{\mathrm{N}}} Ai_{\mathrm{eff}}\sum\Delta\varphi_{\mathrm{Donnan}}dt\right|}{\left(\forall_0^{\mathrm{LC}}c_0^{\mathrm{LC}}-\forall_\theta^{\mathrm{LC}}c_\theta^{\mathrm{LC}}\right)\mathrm{MW}_{\mathrm{NaCl}}} \tag{S12}$$

Membrane ohmic loss, SEC_{s}-MO, is calculated with i_{eff} and the membrane ohmic drops, $\Delta\varphi^{\mathrm{CEM,m}}+\Delta\varphi^{\mathrm{AEM,m}}$:

$$SEC_{\mathrm{s}}\text{-MO}=\frac{\left|\int_0^{t_{\mathrm{N}}} Ai_{\mathrm{eff}}\left(\Delta\varphi^{\mathrm{CEM,m}}+\Delta\varphi^{\mathrm{AEM,m}}\right)dt\right|}{\left(\forall_0^{\mathrm{LC}}c_0^{\mathrm{LC}}-\forall_\theta^{\mathrm{LC}}c_\theta^{\mathrm{LC}}\right)\mathrm{MW}_{\mathrm{NaCl}}} \tag{S13}$$

Channel ohmic loss, SEC_{s}-CO, is calculated with i_{eff} and the two ohmic drops in diluate and concentrate channels, $\Delta\varphi^{\mathrm{HC}}+\Delta\varphi^{\mathrm{LC}}$, as

$$SEC_{\mathrm{s}}\text{-CO}=\frac{\left|\int_0^{t_{\mathrm{N}}} Ai_{\mathrm{eff}}\left(\Delta\varphi^{\mathrm{HC}}+\Delta\varphi^{\mathrm{LC}}\right)dt\right|}{\left(\forall_0^{\mathrm{LC}}c_0^{\mathrm{LC}}-\forall_\theta^{\mathrm{LC}}c_\theta^{\mathrm{LC}}\right)\mathrm{MW}_{\mathrm{NaCl}}} \tag{S14}$$

The rest of the energy is consumed by co-ion currents, i.e., (i–i_{eff}). Current efficiency loss, SEC_{s}-CE, is calculated with i–i_{eff} and the total voltage, ΔV:

$$SEC_{\mathrm{s}}\text{-CE}=\frac{\left|\int_0^{t_{\mathrm{N}}} A(i-i_{\mathrm{eff}})\Delta V dt\right|}{\left(\forall_0^{\mathrm{LC}}c_0^{\mathrm{LC}}-\forall_\theta^{\mathrm{LC}}c_\theta^{\mathrm{LC}}\right)\mathrm{MW}_{\mathrm{NaCl}}} \tag{S15}$$

Summing Eq S12–S15 yields the total SEC_{s} described in the main text (eq 5b).

Here, we discuss the similarities and differences between SEC_{s}-DP and two other energies: 5) energy for overcoming the ideal Nernst potentials, SEC_{s}-IN, and 6) the Gibbs free energy of separation, SEC_{s}-G. The ideal Nernst potential, V_{IN}, is the theoretical electric potential across a perfectly permselective IEM separating the diluate, LC, and the concentrate, HC, streams. V_{IN} between the diluate and concentrate can be expressed as

$$V_{\mathrm{IN}}=-\frac{R_{\mathrm{g}}T}{z_{\mathrm{ct}}F}\ln\left(\frac{\gamma_{\mathrm{ct}}^{\mathrm{HC}}c_{\mathrm{ct}}^{\mathrm{HC}}}{\gamma_{\mathrm{ct}}^{\mathrm{LC}}c_{\mathrm{ct}}^{\mathrm{LC}}}\right) \tag{S16}$$

This theoretical potential is the instantaneous electric voltage to reversibly transfer one counterion between the streams. The energy to overcome the ideal Nernst potential can be estimated as

$$SEC_s\text{-IN} = \frac{\left|\int_0^{t_N} Ai_{\text{eff}}(2V_{\text{IN}})dt\right|}{\left(\forall_0^{\text{LC}} c_0^{\text{LC}} - \forall_\theta^{\text{LC}} c_\theta^{\text{LC}}\right)\text{MW}_{\text{NaCl}}} \quad \text{(S17)}$$

Notably, the absolute value of the ideal Nernst potential is always larger than the sum of the electric potentials at the two membrane-solution interfaces of a practical IEM, since actual IEMs are not ideally permselective (sorbed co-ions lower the voltage at the membrane-solution interfaces down from the theoretical ideal value).[3,9] Therefore, in a membrane pair, $\left|\sum \Delta\varphi_{\text{Donnan}}\right| < 2\left|V_{\text{IN}}\right|$. *SEC*s-DP will be smaller than *SEC*s-IN and approximately equal to *SEC*s-IN when IEM permselectivity approaches 100% (i.e., $\left|\sum \Delta\varphi_{\text{Donnan}}\right| \approx 2\left|V_{\text{IN}}\right|$).

The thermodynamic minimum energy for desalination, *SEC*s-G, is

$$SEC_s\text{-G} = \frac{\Delta G_{\text{sep}}}{\left(\forall_0^{\text{LC}} c_0^{\text{LC}} - \forall_\theta^{\text{LC}} c_\theta^{\text{LC}}\right)\text{MW}_{\text{NaCl}}} \quad \text{(S18)}$$

where ΔG_{sep} is the Gibbs free energy of separation.[21] *SEC*s-IN seemingly equates to *SEC*s-G, as the ideal Nernst potentials ostensibly describe a reversible process for ion transport. However, in *SEC*s-IN, the associated water transport actually renders the process thermodynamically irreversible. Therefore, *SEC*s-IN includes an irreversible energy cost for water transport and would be larger than *SEC*s-G. In addition, we clarify that V_{IN} is the ideal Nernst potential and not the membrane potential measured in apparent permselectivity characterizations. The latter includes the effects of water transport and co-ion leakage, whereas the ideal Nernst potential does not have either effects.[17]

For the simulation of desalinating 1.0 M feeds in Figure 4, the *SEC*s-DP, *SEC*s-IN, and *SEC*s-G are 14.0, 21.3, and 17.0 Wh/kg-NaCl, respectively. *SEC*s-DP < *SEC*s-IN, due to the nonideal permselectivity, and *SEC*s-IN > *SEC*s-G, due to the irreversible water transport. The differences between *SEC*s-DP, *SEC*s-IN, and *SEC*s-G vanishes if the permselectivity is very high and water transport is insignificant. For example, in the desalination of 0.20 M feeds to 0.10 M, *SEC*s-DP, *SEC*s-IN, and *SEC*s-G converges to approximately the same value (10.3, 11.0 and 11.0 Wh/kg-NaCl, respectively).

Maximum Water Recovery Yield. An upper concentration limit of the effluent concentrate, c_{lim}, can be determined by current density and diluate concentration. Here, a method to estimate maximum water recovery yield, Y_{lim}, with c_{lim} is presented. The initial feed concentration is c_{o}, and the target product concentration is set as c^{target}. c_{lim} is calculated with c^{target} as the effluent diluate concentration. The maximum recovery yield is achieved when the diluate is desalinated to c^{target} and the concentrate salinity is raised to c_{lim}. To avoid the influence of mass density changes, molar concentrations are converted into mass fractions of salts, i.e., $x_{\mathrm{o}}^{\mathrm{s}}$, $x_{\mathrm{lim}}^{\mathrm{s}}$ and $x^{\mathrm{s,target}}$ (mass density data for the conversion can be found in literature)[22]. Masses of the final diluate and concentrate solutions are denoted by M_{LC} and M_{HC}, respectively. Mass of the initial influent feed solution is, thus, M_{LC}+M_{HC} (Figure 1A and B of the main manuscript). The mass conservation of salts dictates

$$(M_{\mathrm{LC}} + M_{\mathrm{HC}})x_{\mathrm{o}}^{\mathrm{s}} = M_{\mathrm{HC}}x_{\mathrm{lim}}^{\mathrm{s}} + M_{\mathrm{LC}}x^{\mathrm{s,target}} \tag{S19}$$

which can be rearranged as

$$M_{\mathrm{LC}} = \frac{x_{\mathrm{lim}}^{\mathrm{s}} - x_{\mathrm{o}}^{\mathrm{s}}}{x_{\mathrm{o}}^{\mathrm{s}} - x^{\mathrm{s,target}}} M_{\mathrm{HC}} \tag{S20}$$

The mass densities of initial feed and final diluate are $\rho(x_{\mathrm{o}}^{\mathrm{s}})$ and $\rho(x^{\mathrm{s,target}})$. The volumes of initial feed and final diluate can be expressed as $M_{\mathrm{LC}} \Big/ \rho\left(x^{\mathrm{s,target}}\right)$ and $(M_{\mathrm{HC}} + M_{\mathrm{LC}}) \Big/ \rho\left(x_{\mathrm{o}}^{\mathrm{s}}\right)$, respectively. Combining the volume expressions with eq S20 and rearranging gives the maximum water recovery yield:

$$\begin{aligned} Y_{\mathrm{lim}} &= \frac{M_{\mathrm{LC}} \Big/ \rho\left(x^{\mathrm{s,target}}\right)}{\left(M_{\mathrm{HC}} + M_{\mathrm{LC}}\right) \Big/ \rho\left(x_{\mathrm{o}}^{\mathrm{s}}\right)} = \frac{\left(\dfrac{x_{\mathrm{lim}}^{\mathrm{s}} - x_{\mathrm{o}}^{\mathrm{s}}}{x_{\mathrm{o}}^{\mathrm{s}} - x^{\mathrm{s,target}}}\right) \Big/ \rho\left(x^{\mathrm{s,target}}\right)}{\left(1 + \dfrac{x_{\mathrm{lim}}^{\mathrm{s}} - x_{\mathrm{o}}^{\mathrm{s}}}{x_{\mathrm{o}}^{\mathrm{s}} - x^{\mathrm{s,target}}}\right) \Big/ \rho\left(x_{\mathrm{o}}^{\mathrm{s}}\right)} \\ &= \frac{\left(x_{\mathrm{lim}}^{\mathrm{s}} - x_{\mathrm{o}}^{\mathrm{s}}\right) \Big/ \rho\left(x^{\mathrm{s,target}}\right)}{\left(x_{\mathrm{lim}}^{\mathrm{s}} - x^{\mathrm{s,target}}\right) \Big/ \rho\left(x_{\mathrm{o}}^{\mathrm{s}}\right)} \end{aligned} \tag{S21}$$

Simulation at the Module Scale. In this study, the desalination performance of the ED stack is simulated by numerical integration of species transfers across a membrane pair over small time-steps (1.0 s). The equations are computed using Python code. The exiting streams are

immediately recirculated back to the stack (i.e., recirculation time outside the stack is negligible) operates at fast virtual recirculation. In a cell pair of the stack, the effective membrane size, *A*, is 1.0 m^2, and the thickness of each fluid channel is 1.0 mm. The total volumes recirculated in the channels ($\forall_0^{LC}$ and $\forall_0^{HC}$) are initiated at 1.0 m^3, for the analyses where diluate and concentrate are injected with the same volume. For the analyses presented in Figures 4 and 5, which examine different water recovery yields, $\forall_0^{LC}$ are adjusted according to the different volumetric ratios.

The governing mass balance in the stack can be expressed as:

$$\frac{\partial c_i}{\partial t} + \nabla \cdot J_i = 0 \tag{S22}$$

This study focuses on the insights into membrane development rather than stack design. Therefore, the flow paths in the diluate and concentrate channels are not discretized. The ion transport can be further expressed as

$$\frac{\Delta c_{Na}^{LC}}{\Delta t} + \frac{A(J_{Na}^{CEM} - J_{Na}^{AEM})}{\forall^{LC}} = 0 \tag{S23}$$

$$\frac{\Delta c_{Na}^{HC}}{\Delta t} - \frac{A(J_{Na}^{CEM} - J_{Na}^{AEM})}{\forall^{HC}} = 0 \tag{S24}$$

The Cl concentrations in the two chambers are the same as the Na concentrations due to charge neutrality. The mass of water permeated across the membrane, ΔM , can be calculated with

$$\frac{\Delta M}{\Delta t} - A(\left|J_W^{CEM}\right| + \left|J_W^{AEM}\right|)\rho_{water} = 0 \tag{S25}$$

In the next time-step (i.e., 1.0 s), the concentration changes are determined by Δc_{Na} and the volume changes of $\forall^{LC}$ and $\forall^{HC}$ are computed using $\Delta M \Delta t$ and the density of saline water. In addition, assume linear concentration gradient and electrical potential gradient are assumed in the IEMs to reduce the computation workload. Eq 1 of the main manuscript is essentially computed in the program as

$$J_i = -D_i^m \frac{\Delta c_i^m}{\Delta x} - D_i^m c_i^m \frac{z_i F}{R_g T} \frac{\Delta \varphi^m}{\Delta x} \tag{S26}$$

The simulation proceeds until the diluate concentration reaches the target product stream salinity of 0.10 M NaCl (unless specified otherwise). Performance metrics, *SEC*, *Y*, and *SR*, are calculated using the appropriate equations in the main text and SI.

RESULTS AND DISCUSSION

Operation with Different Current Densities To investigate the influence of applied current density, *i*, on desalination, electric currents of 5.0–40 mA/cm^2 are applied to the same ED model setup, i.e., simulated membrane properties of $c_{\text{fix}}^{\text{m}}$ = 1.5 equiv/L, f_{w} = 0.25, and Δx = 100 μm and channel distance of 1.0 mm. The concentrations of diluate and concentrate influents are initialized as 1.0 M, and the target product concentration of the effluent diluate is set as 0.10 M.

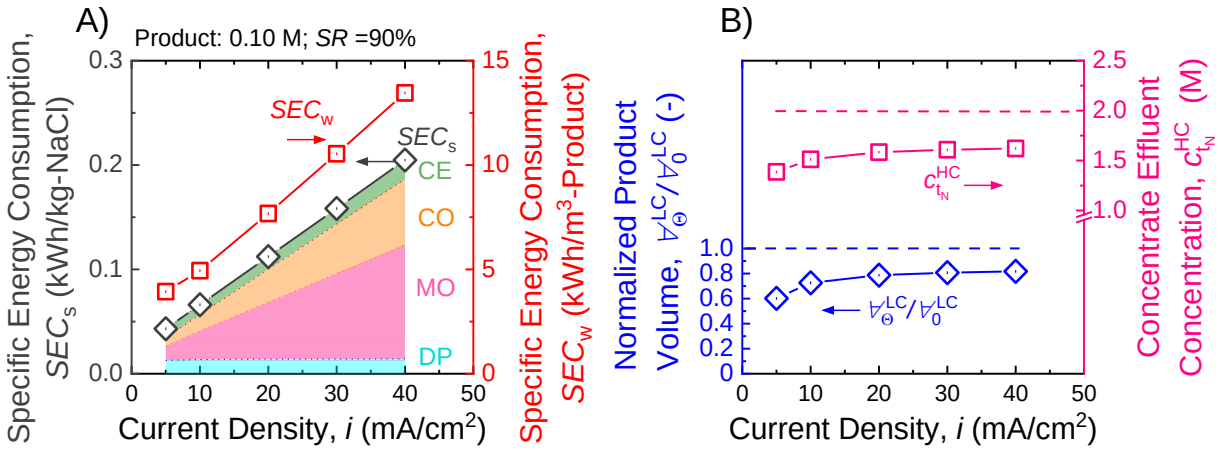

Figure S4. A) Specific energy consumption of desalination, normalized by salt removal, SEC_{s}, and product stream, SEC_{w}, as functions of applied current density, *i*. SEC_{s}, denoted by black diamond symbols (left vertical axis), is further decomposed into the energy costs of overcoming the Donnan potentials (blue region), ohmic loss of membranes (pink region), ohmic loss of channels (orange region), and compensating for imperfect permselectivity (green region). SEC_{w} is represented by red square symbols (right vertical axis). B) Volume of product (i.e., diluate effluent) stream normalized by initial volume, $\forall_{\theta}^{\text{LC}} / \forall_{0}^{\text{LC}}$, and concentration of concentrate effluent, $c_{t_{\text{N}}}^{\text{HC}}$, in ED desalination under different applied current densities, *i*. Blue diamond and pink square symbols denote $\forall_{\theta}^{\text{LC}} / \forall_{0}^{\text{LC}}$ and $c_{t_{\text{N}}}^{\text{HC}}$, respectively (left and right vertical axes). Dashed lines indicate the quantities assuming no transmembrane water transport. The simulated ED processes operate with equal volumes of diluate and concentrate influents and reduced the diluate salinity from 1.0 M to 0.10 M. Membrane properties of $c_{\text{fix}}^{\text{m}}$ = 1.5 equiv/L, f_{w} = 0.25, Δx = 100 μm and stack channel distance of 1.0 mm were adopted.

SEC_s is nearly linear with respect to applied current density, ascending from 43.1 to 205 Wh/kg-NaCl as i increases from 5.0 to 40 mA/cm^2 (black diamond symbols of Figure S4A). The linearity can be intuitively attributed to Ohm's law. The ohmic losses of membrane and channel resistance dominate the energy consumption, thus, yielding $\Delta SEC_s \propto \left(i^2 Rt\right)/n_{salt}$. Here, R is the total ohmic resistance across the stack, t is the desalination time, and n_{salt} is the moles of salts separated from the diluate. As permselectivity approaches ideal, $it \approx n_{salt}F$ and ΔSEC_s is approximately proportional to iR. R does substantially change for different desalinations with the same initial and final feed and outlet concentrations. Therefore, ΔSEC_s is effectively proportional to the applied current density, i.

The energy consumption can be broken down into its four constituents: work required to overcome the Donnan potentials, membrane ohmic loss, channel ohmic loss, and current efficiency loss, represented in Figure S4A as the blue, pink, orange, and green regions respectively. The membrane ohmic loss increases from 12.8 to 109 Wh/kg-NaCl, while the channel ohmic loss rises from 7.69 to 63.3 Wh/kg-NaCl. In contrast, the energy cost for overcoming the Donnan potentials does not significantly change (12.8 to 14.2 Wh/kg-NaCl). The current efficiency loss increases from 8.92 to 18.2 Wh/kg-NaCl as a larger electric current is applied, but its relative contribution to the SEC_s drops from 21% to 9%. This is because, under a smaller applied current, concentration gradient-driven diffusion resulted in the elevated importance of co-ion fluxes, which consequently yields a larger ratio of current efficiency loss to the overall energy cost.[6] .The energy consumption normalized by product volume, SEC_w, shadows the quasi-linear trend of SEC_s-i, rising from 3.93 to 13.5 kWh/m^3-product (red square symbols). Notably, at low i (i.e., leftmost data points), the SEC_w is significantly impacted by the greater water loss from the diluate stream.

In Figure S4B, as the applied current density increases from 5.0–40 mA/cm^2, the normalized (dimensionless) product volume, $\forall_\theta^{LC}/\forall_0^{LC}$, rises from 0.602 to 0.817. Lower current densities lengthen the duration of desalination to reach the target product water salinity, resulting in more water transport. Increasing the current density improves $\forall_\theta^{LC}/\forall_0^{LC}$ but does not raise $\forall_\theta^{LC}/\forall_0^{LC}$ to 1.0. Instead, $\forall_\theta^{LC}/\forall_0^{LC}$ asymptotes at ≈0.80. The unavoidable ≈20% volume loss is due to electro-osmosis, where water molecules are dragged across the IEMs by the permeating ions. This volume reduction is determined by the electro-osmotic coefficient, P_w^E , and scales with

Δc^{LC}. The impacts of electro-osmosis on desalination performance are further analyzed later. Operating at higher current densities reduces the diluate volume loss and increases the concentrate effluent concentration from 1.39 to 1.62 M. Therefore, a higher current density can enhance product water yield, minimize concentrate effluent volume, and achieve higher concentrate effluent salinity (Figure S4B), but the performance improvements are at the expense of greater energy cost (Figure S4A).

The above analyses show that the applied current density is a critical operating parameter influencing hypersaline ED performance as i determines SEC_s, SEC_w, water recovery yield, and concentrate effluent salinity. Lower I reduces desalination energy cost by suppressing the ohmic energy loss but would suffer a detrimental loss of product water. In addition, operating at lower current densities would require a larger membrane area to obtain the same desalination capacity (reciprocal relationship between current density and membrane area), thereby increasing the capital cost. Overall, the feasibility of cost savings with smaller electric currents is likely to be limited.

Upper Limits of Concentrate Effluent Concentration are Determined by Applied Current Density. Figures S5A and B display the concentrations and volumes, respectively, of diluate and concentrate channels (corresponding to dashed and solid lines) as functions of time for the desalination of 1.5 M feeds to 0.10 M. Note that a higher feed salinity (than the 1.0 M in the previous simulations) was adopted to accentuate and highlight the water transport issues. As the electrodialysis progresses, the diluate concentrations gradually drop to 0.10 M and the concentrate salinities rise correspondingly but level off after some time. This plateauing is particularly prominent for the lower current densities of 10 and 20 mA/cm^2 (blue and green solid lines). Applying larger currents (increasing from 10 to 40 mA/cm^2) can elevate the plateau concentrations from ≈1.9 to >2.2 M as smaller volumes of water are transported from the diluate to concentrate streams (deviations of dashed and solid lines from the horizontal black line in Figure S5B). Hence, the upper concentration limit of the concentrate can be raised by higher applied currents.

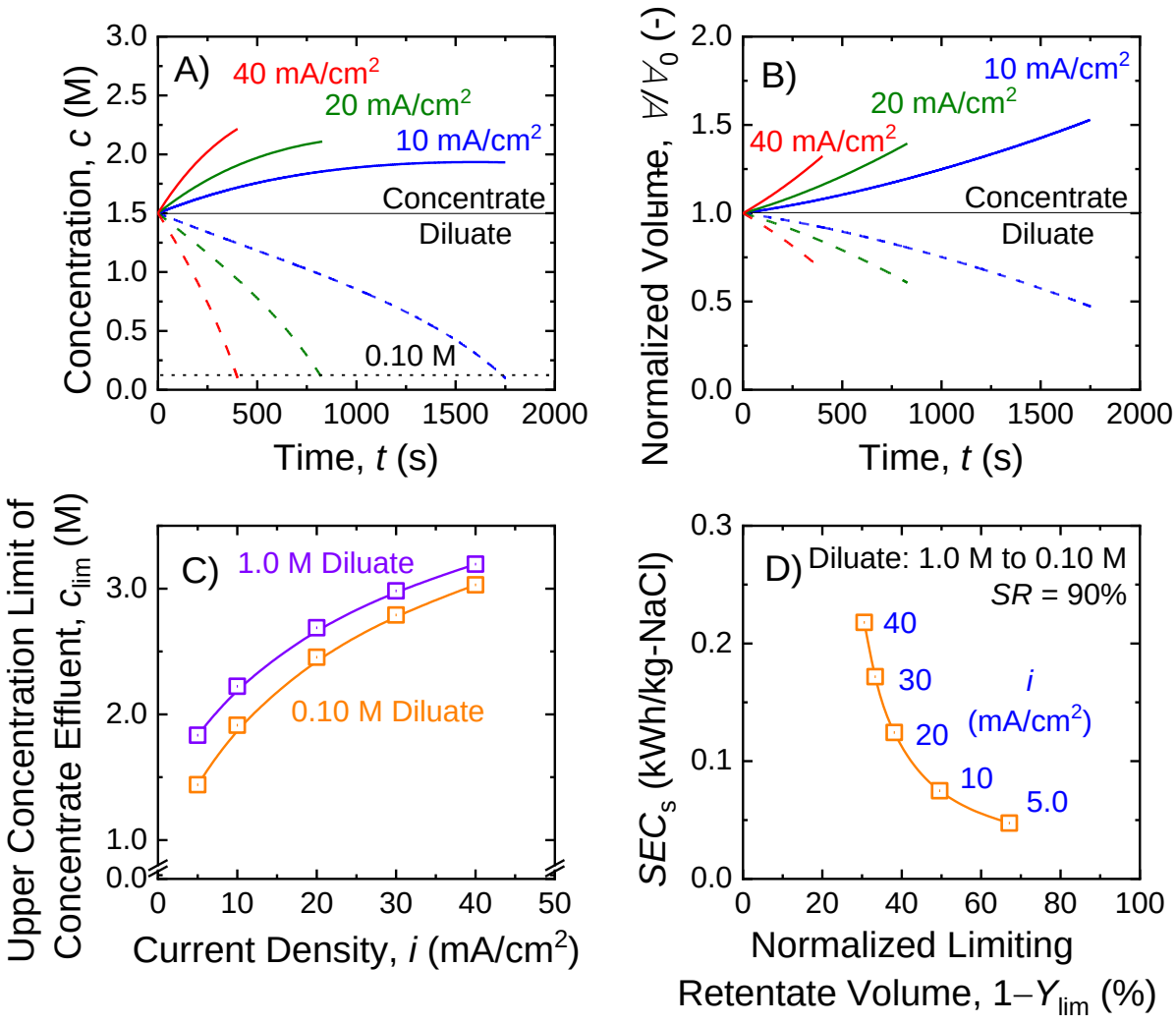

Figure S5. A) Concentrations, c, and B) normalized volumes, $\forall / \forall_0$, as functions of time for desalinating 1.5 M feeds to 0.10 M. Blue, green, and red lines represent operation at 10, 20, and 40 mA/cm^2, respectively, while dashed and solid lines denote diluate and concentrate streams, respectively. Horizontal black lines indicate initial values. C) Upper concentration limit of concentrate effluent, c_{lim}, as a function of applied current density, i, for exiting diluate concentrations of 0.10 M (orange squares) and 1.0 M (orange and violet square symbols, respectively). The simulations were carried out with initial feed salinity of 1.5 M. D) Tradeoff relationship between normalized limiting retentate volume, $1-Y_{\text{lim}}$, and specific energy consumption of salt removal, SEC_s, for desalinating 1.0 M feeds to 0.10 M. Membrane properties of $c_{\text{fix}}^{\text{m}}$ = 1.5 equiv/L, f_w = 0.25, and Δx = 100 μm and stack channel distance of 1.0 mm were adopted.

These concentration plateaus can be quantitatively understood by considering salt and water across the IEMs. Using a 1:1 salt (e.g., NaCl) to illustrate, the net salt flux, J_s, from diluate

to concentrate can be represented by $J_{ct}^{CEM} - J_{co}^{AEM}$, which is the counterion flux across the CEM subtracting the co-ion leakage across the AEM (based on charge balance, utilizing the anionic fluxes, i.e., $J_{co}^{CEM} - J_{ct}^{AEM}$, yields the same J_s). The net salt flux can be described by $\left(T_{ct}^{CEM} - T_{co}^{AEM}\right) i \big/ z_i F$, where T is the transport number of the cationic charge carriers. Meanwhile, water permeating across the CEM and AEM accumulates in the concentrate channel and the total water flux, J_w, is $\left|J_w^{CEM}\right| + \left|J_w^{AEM}\right|$. The salt and water transports can be jointly considered as the permeation of an equivalent salt solution of concentration J_s/J_w from the diluate to the concentrate. If J_s/J_w is lower than the concentration in the concentrate channel, the concentrate solution would be diluted. Therefore, as the desalination progresses, the concentration of the concentrate channel eventually reaches a limiting level, c_{lim}. c_{lim} can be described eq 8 in the main text or rearranged as eq S27:

$$c_{lim} = \left.\frac{J_s}{J_w}\right|_{lim} = \left.\frac{J_{ct}^{CEM} - J_{co}^{AEM}}{\left|J_w^{CEM}\right| + \left|J_w^{AEM}\right|}\right|_{lim} = \left.\frac{T_{ct}^{CEM} - T_{co}^{AEM}}{\left|J_w^{CEM}\right| + \left|J_w^{AEM}\right|}\right|_{lim} \frac{i}{z_i F} \tag{S27}$$

The desalination of the diluate stream is separate and independent from the concentrate stream reaching c_{lim}. As long as the diluate concentration is less than J_s/J_w, the diluate concentration would continue to drop, although more product volume would be lost.

Eq S27 indicates that higher current densities, i, can substantially raise c_{lim}, leading to the higher concentration plateaus in Figure S5A. Figure S5C further demonstrates the influence of i on c_{lim}. When the effluent diluate concentration is set as 0.10 M, c_{lim} increases from 1.44 to 3.03 M as i rises from 5.0 to 40 mA/cm^2. Increasing the diluate concentration to 1.0 M, elevates c_{lim} to 1.84–3.19 M across the i range. The higher diluate concentration narrows the osmotic pressure difference between the diluate and concentrate channels and reduces osmotic water fluxes, thus, allowing a higher c_{lim} in the concentrate channel. However, compared to the 0.90 M increase in the diluate, the gains in c_{lim} are only 0.2–0.4 M because the higher concentrations in these channels compromised the IEM permselectivities and lessened $T_{ct}^{CEM} - T_{co}^{AEM}$ in eq S27.

The highest water recovery yield that the electrodialysis stack can achieve occurs when the concentrate effluent reaches the maximum concentration c_{lim}. These maximum Ys correspond to the asymptotic water recovery yields of SEC_w-Y curves in Figure S5A of the main manuscript. A

higher current density can raise c_{lim} to produce a more saline concentrate effluent and simultaneously achieve a higher Y. Further examination of the relationship between c_{lim} and the influent feed salinity reveals a second insight: because feed concentrations that exceed c_{lim} would not have meaningful water recovery yields, c_{lim} is also the upper limit for the feed salinity that can be desalinated in hypersaline electrodialysis.

The analyses of c_{lim} above imply an i-directed tradeoff relationship between SEC and Y. Increasing current density leads to a higher c_{lim} and a larger obtainable Y but would be more energy-intensive as the ohmic energy loss increases. Figure S5D demonstrates this tradeoff relationship. The normalized limiting retentate volume, $1-Y_{lim}$, is plotted as a function of SEC_s for desalinating 1.0 M feeds to 0.10 M. SEC_s increases from 47.4 to 218 Wh/kg-NaCl as the normalized limiting retentate volume increases from 30.6% to 67.1%. Although lower current densities require advantageously low SEC_ss, the application of such minute ionic fluxes in hypersaline ED is unlikely to be practical as the exacerbated water transport would drastically reduce recovery yields.

Model Validation. Permselectivities and conductivities of membranes with fixed charge density of 1.0 and 1.5 equiv/L with simulated using the model (solid lines of Figure S6) and compared against experimental measurements of poly(phenylene oxide) membranes with the same range of fixed charge density (red circle symbols). The simulation conditions are 0.10 M in the diluate and 0.50 M in the concentrate to match the conditions of the experimental measurements. The experimental values fall within the ranges of α and σ^m modeled, signifying that the elementary component of the model, the IEMs, can be described by the governing transport equations (eq 1 and eqs S1–7).

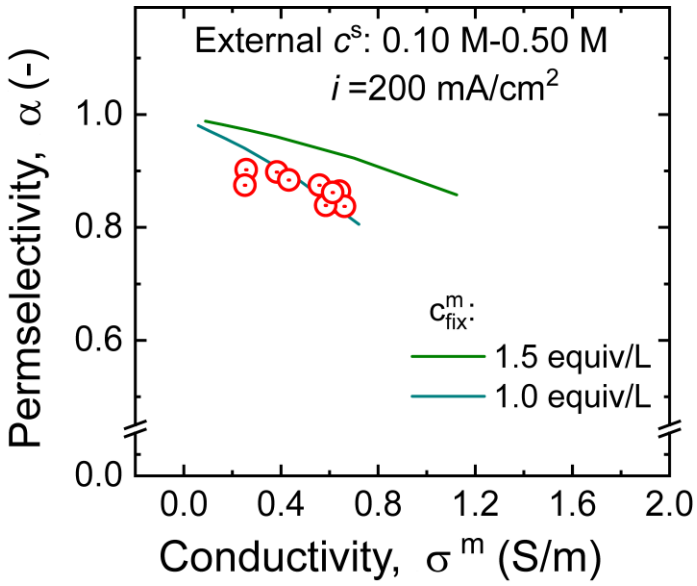

Figure S6. Comparison of simulated permselectivity-conductivity trends (solid lines) to experimental data (red circle symbols)[23] of sulfonated poly(phenylene oxide) membranes.

Supplementary Tables

Table S1. Parameters and variables used in the study, with the values of constants and empirical parameters listed where applicable

Symbol	Description	Unit and value
α	Permselectivity	-
γ	Activity coefficient	-
ε_0	Permittivity of vacuum	8.854×10^{-12} F/m
ε_r	Relative permittivity	-
θ	Hydraulic retention time	s
φ	Potential	V
$\Delta\varphi_{\text{Donnan}}$	Donnal potential	V
λ	Number of sorbed water molecules per fixed charge site	-
ξ	Manning parameter	-
$\Delta\pi$	Osmotic pressure difference	Pa
ρ	Density of solution	kg/m^3
σ^{m}	Membrane conductivity	S/m
φ	Potential	V
A	Membrane area	1.0 m^2
c	Concentration	M
c^{target}	Target product concentration	0.10 M
c_{ct}^{m}	Membrane counterion concentration (per volume of hydrated membrane)	M
c_{co}^{m}	Membrane co-ion concentration (per volume of hydrated membrane)	M

c_{fix}^{m}	Membrane fixed charge density (per volume of hydrated membrane)	equiv/L
c_{lim}	Limiting concentration	M
D^{m}	Effective ion diffusivity within the membrane	m^2/s
$D_{ct,u}^{m}$	Uncondensed counterion diffusivity in membrane	m^2/s
$D_{ct,c}^{m}$	Condensed counterion diffusivity in membrane	m^2/s
D_{Na}^{s}	Bulk sodium ion diffusivity	1.334×10^{-9} m^2/s
D_{Cl}^{s}	Bulk chloride ion diffusivity	2.032×10^{-9} m^2/s
e	Elementary charge	1.602×10^{-19} C
f_w	Volume fraction of water in membrane	-
f_u	Fraction of counterions in the membrane that are uncondensed	-
F	Faraday's constant	96,485 C/mol
i	Current density	mA/cm^2
J_i	Molar flux of ion, i	$mol/m^2/s$
J_w	Water flux	m/s
J_w^O	Osmotic water flux	m/s
J_w^E	Electro-osmotic water flux	m/s
k_B	Boltzmann's constant	1.380×10^{-23} J/K
M	Mass	Kg
MW_{NaCl}	Molecular weight of NaCl	58.44 g/mol
n_1	Fitting parameter 1 in the Yasuda model	0.3995
n_2	Fitting parameter 2 in the Yasuda model	2.850
n_3	Fitting parameter 3 in the Yasuda model	3.029

N_A	Avogadro's constant	6.022×10^{23} mol^{-1}
P_w^O	Osmotic water permeability	m^2/s/Pa or μm·L/m^2/h/bar
P_w^E	Electro-osmotic water permeability	7.12×10^{-10} m^3 A^{-1} s^{-1}
R_g	The gas constant	8.314 J/mol/K
SEC_s	Specific energy consumption (normalized by mass of salts separated)	kWh/kg-NaCl
SEC_w	Specific energy consumption (normalized by product stream volume)	kWh/m^3
SR	Salt removal	-
t	Time	s
T	Absolute temperature	298 K
T_i	Transport number of ion, i	-
V	Voltage	V
V_{IN}	Ideal Nernst potential	V
x	Position in the direction normal to the membrane surface	m
$\Delta x^{LC/HC}$	Channel thickness	0.0010 m
x^s	mass fraction of salt in solution	-
X	Ratio of fixed charge density to membrane co-ion concentration in the Manning model	-
Y	Water recovery yield	-
Y_{lim}	Limiting water recovery yield	
z	Ion valence	-
$\forall$	Volume of fluid	m^3

Table S2. Definitions of the acronyms, superscripts, and subscripts used in the nomenclature of this study.

Symbol	Description
AEM	Anion exchange membrane
co	Co-ion
ct	Counterion
CEM	Cation exchange membrane
ED	Electrodialysis
HSED	Hypersaline electrodialysis
HC	High concentration, or concentrate chamber
IEM	Ion-exchange membrane
LC	Low concentration, or diluate chamber
m	Membrane
s	Bulk solution

REFERENCES

(1) Kamcev, J.; Galizia, M.; Benedetti, F. M.; Jang, E.-S.; Paul, D. R.; Freeman, B. D.; Manning, G. S. Partitioning of Mobile Ions between Ion Exchange Polymers and Aqueous Salt Solutions: Importance of Counter-Ion Condensation. *Phys. Chem. Chem. Phys.* **2016**, *18* (8), 6021–6031. https://doi.org/10.1039/C5CP06747B.

(2) Kamcev, J.; Paul, D. R.; Freeman, B. D. Ion Activity Coefficients in Ion Exchange Polymers: Applicability of Manning's Counterion Condensation Theory. *Macromolecules* **2015**, *48* (21), 8011–8024. https://doi.org/10.1021/acs.macromol.5b01654.

(3) Strathmann, H. *Ion-Exchange Membrane Separation Processes*; Elsevier, 2004.

(4) Pitzer, K. S. Thermodynamics of Electrolytes. I. Theoretical Basis and General Equations. *J. Phys. Chem.* **1973**, *77* (2), 268–277. https://doi.org/10.1021/j100621a026.

(5) Pitzer, K. S.; Mayorga, G. Thermodynamics of Electrolytes. II. Activity and Osmotic Coefficients for Strong Electrolytes with One or Both Ions Univalent. *J. Phys. Chem.* **1973**, *77* (19), 2300–2308. https://doi.org/10.1021/j100638a009.

(6) Luo, T.; Abdu, S.; Wessling, M. Selectivity of Ion Exchange Membranes: A Review. *Journal of Membrane Science* **2018**, *555*, 429–454. https://doi.org/10.1016/j.memsci.2018.03.051.

(7) Kamcev, J.; Paul, D. R.; Manning, G. S.; Freeman, B. D. Ion Diffusion Coefficients in Ion Exchange Membranes: Significance of Counterion Condensation. *Macromolecules* **2018**, *51* (15), 5519–5529. https://doi.org/10.1021/acs.macromol.8b00645.

(8) Vanysek, P. Ionic Conductivity and Diffusion at Infinite Dilution. *CRC handbook of chemistry and physics* **2000**, *83*, 76–78.

(9) Fan, H.; Yip, N. Y. Elucidating Conductivity-Permselectivity Tradeoffs in Electrodialysis and Reverse Electrodialysis by Structure-Property Analysis of Ion-Exchange Membranes. *J. Membr. Sci.* **2019**, *573*, 668–681. https://doi.org/10.1016/j.memsci.2018.11.045.

(10) Huang, Y.; Fan, H.; Yip, N. Y. Mobility of Condensed Counterions in Ion-Exchange Membranes: Application of Screening Length Scaling Relationship in Highly Charged Environments. *Environ. Sci. Technol.* **2024**, *58* (1), 836–846. https://doi.org/10.1021/acs.est.3c06068.

(11) Bard, A. J.; Faulkner, L. R. *Electrochemical Methods: Fundamentals and Applications*, 2nd ed.; Wiley: New York, 2001.

(12) Yasuda, H.; Lamaze, C. E.; Peterlin, A. Diffusive and Hydraulic Permeabilities of Water in Water-Swollen Polymer Membranes. *Journal of Polymer Science Part A-2: Polymer Physics* **1971**, *9* (6), 1117–1131. https://doi.org/10.1002/pol.1971.160090608.

(13) Xie, W.; Cook, J.; Park, H. B.; Freeman, B. D.; Lee, C. H.; McGrath, J. E. Fundamental Salt and Water Transport Properties in Directly Copolymerized Disulfonated Poly(Arylene Ether Sulfone) Random Copolymers. *Polymer* **2011**, *52* (9), 2032–2043. https://doi.org/10.1016/j.polymer.2011.02.006.

(14) Luo, H.; Aboki, J.; Ji, Y.; Guo, R.; Geise, G. M. Water and Salt Transport Properties of Triptycene-Containing Sulfonated Polysulfone Materials for Desalination Membrane Applications. *ACS Appl. Mater. Interfaces* **2018**, *10* (4), 4102–4112. https://doi.org/10.1021/acsami.7b17225.

(15) Kimura, S. Reverse Osmosis Performance of Sulfonated Poly (2, 6-Dimethylphenylene Ether) Ion Exchange Membranes. *Industrial & Engineering Chemistry Product Research and Development* **1971**, *10* (3), 335–339.

(16) Paul, M.; Park, H. B.; Freeman, B. D.; Roy, A.; McGrath, J. E.; Riffle, J. S. Synthesis and Crosslinking of Partially Disulfonated Poly(Arylene Ether Sulfone) Random Copolymers as Candidates for Chlorine Resistant Reverse Osmosis Membranes. *Polymer* **2008**, *49* (9), 2243–2252. https://doi.org/10.1016/j.polymer.2008.02.039.

(17) Kingsbury, R. S.; Coronell, O. Modeling and Validation of Concentration Dependence of Ion Exchange Membrane Permselectivity: Significance of Convection and Manning's Counter-Ion Condensation Theory. *Journal of Membrane Science* **2021**, *620*, 118411. https://doi.org/10.1016/j.memsci.2020.118411.

(18) Kamcev, J. Ion Sorption and Transport in Ion Exchange Membranes: Importance of Counter-Ion Condensation. **2016**.

(19) Cook, J. R. Fundamental Water and Ion Transport Characterization of Sulfonated Polysulfone Desalination Materials. **2014**.

(20) Tanaka, Y. Mass Transport and Energy Consumption in Ion-Exchange Membrane Electrodialysis of Seawater. *Journal of Membrane Science* **2003**, *215* (1), 265–279. https://doi.org/10.1016/S0376-7388(03)00020-6.

(21) Shah, K. M.; Billinge, I. H.; Chen, X.; Fan, H.; Huang, Y.; Winton, R. K.; Yip, N. Y. Drivers, Challenges, and Emerging Technologies for Desalination of High-Salinity Brines: A Critical Review. *Desalination* **2022**. https://doi.org/10.1016/j.desal.2022.115827.

(22) Perry, J. H. *Chemical Engineers' Handbook*, 8th ed.; McGraw-Hill., 2008.

(23) Fan, H.; Huang, Y.; Yip, N. Y. Advancing the Conductivity-Permselectivity Tradeoff of Electrodialysis Ion-Exchange Membranes with Sulfonated CNT Nanocomposites. *Journal of Membrane Science* **2020**, *610*, 118259. https://doi.org/10.1016/j.memsci.2020.118259.